Zhi et al. Nanoscale Research Letters (2017) 12:632
DOI 10.1186/s11671-017-2391-3

Nanoscale Research Letters

NANO EXPRESS Open Access

Perovskite Solar Cells Fabricated by Using an Environmental Friendly Aprotic Polar Additive of 1,3-Dimethyl-2-imidazolidinone

Lili Zhi[1,2], Yanqing Li[2], Xiaobing Cao[3,4,5], Yahui Li[3,4,5], Xian Cui[3,4,5], Lijie Ci[1*] and Jinquan Wei[3,4,5*]

Abstract

Perovskite solar cells (PSCs) have great potentials in photovoltaics due to their high power conversion efficiency and low processing cost. PSCs are usually fabricated from PbI_2/dimethylformamide solution with some toxic additives, such as *N*-methyl pyrrolidone and hexamethylphosphoramide. Here, we use an environmental friendly aprotic polar solvent, 1,3-dimethyl-2-imidazolidinone (DMI), to fabricate perovskite films. By adding 10 vol% DMI in the precursor solution, high-quality perovskite films with smooth surface are obtained. By increasing annealing temperature from 100 to 130 °C, the average grain size of the perovskite increases from ~ 216 to 375 nm. As a result, the efficiency of the PSCs increases from 10.72 to 14.54%.

Keywords: Perovskite solar cell, Aprotic polar solvent, Lewis acid–base adduct, 1,3-Dimethyl-2-imidazolidinone

Background

Recently, organometallic halide perovskite solar cells (PSCs) have attracted great attentions due to rapid growth of power conversion efficiency (PCE) and low processing cost [1–8]. Currently, the perovskite solar cells are mainly fabricated through solution-based processing, including one-step [9–12], two-step [13, 14], and additive-assisted deposition methods [15, 16]. The two-step method has been widely used for achieving high-efficient perovskite solar cells. In the traditional two-step method, the $CH_3NH_3PbI_3$ perovskite ($MAPbI_3$) is formed through intercalation of CH_3NH_3I (MAI) into the PbI_2 lattice, which usually leads to rough surface due to volume expansion and existence of some small grains on the perovskite films [17, 18].

Generally, dimethylformamide (DMF) is used as solvent for preparing PbI_2 and $MAPbI_3$ films. The volatile DMF solvent has a high saturated vapor pressure, which makes the PbI_2 crystallize rapidly during spin-coating of the PbI_2/DMF solution, so it is hard to control the crystallinity of the PbI_2 films. The morphology of the perovskite film depends on the PbI_2 strongly. In order to obtain smooth and dense perovskite films with large grains, researchers usually added some additives to the PbI_2/DMF precursor solution. For example, Zhang et al. reported preparation of a smooth $MAPbI_3$ film by incorporating 4-tert-butylpyridine (TBP) into the PbI_2/DMF precursor solution [19]. Li et al. mediated the nucleation and grain growth pathway to obtain large perovskite grains in micrometer scale by introducing an acetonitrile to the PbI_2/DMF solution [20]. Recently, Lewis acid–base adduct approach was also used to fabricate high-quality perovskite films. Some aprotic polar solvents, such as DMF, *N*,*N*-dimethyl sulfoxide (DMSO), *N*-methyl pyrrolidone (NMP), and hexamethylphosphoramide (HMPA), have been used as Lewis base solvents to improve the quality and performance of the perovskite solar cells [21–23]. Lee et al. [24] pointed out that aprotic polar solvents, containing oxygen, sulfur, or nitrogen ligands, were Lewis bases, which can form Lewis acid–base adducts of PbI_2·xSol with PbI_2 through dative bonds. The Lewis adducts of PbI_2·xSol lead to high-quality perovskite films and high-efficient PSCs. However, the above aprotic polar solvents are toxic, which harm health and environments.

1,3-Dimethyl-2-imidazolidinone (DMI) is also an aprotic polar solvent with low volatility. The DMI has a five-membered ring and a carbonyl (see Additional file 1: Figure S1). Due to the isolated electron pair on the O

* Correspondence: lci@sdu.edu.cn; jqwei@tsinghua.edu.cn
[1]School of Materials Science and Engineering, Shandong University, Jinan 250061, Shandong, People's Republic of China
[3]Key Lab for Advanced Materials Processing Technology of Education Ministry, Tsinghua University, Beijing 100084, People's Republic of China
Full list of author information is available at the end of the article

atom of the carbonyl, DMI can also form a Lewis adduct with PbI_2. More importantly, the potential toxicological risk of DMI is less than carcinogen HMPA and reproductive toxicity NMP. Thus, it is a good alternative solvent to the HMPA and NMP, in forming perovskite through the Lewis adduct approach because it provides a safer working environment [25]. Here, we introduce the DMI solvent into the PbI_2/DMF precursor solution to improve quality of the perovskite films.

Methods

Device Fabrication

The perovskite films and solar cells were fabricated by a modified two-step method, which has been reported in details in our previous paper [22]. In brief, a compact TiO_2 blocking layer was spin-coated a mildly acidic solution of titanium isopropoxy solution in ethanol at 2000 rpm for 30 s on FTO substrate, followed by sintering at 500 °C for 30 min. A mesoporous TiO_2 layer was then deposited on the blocking layer by spin-coating diluted TiO_2 paste (Dyesol-30NRT, Dyesol) in ethanol (1:6, weight ratio) at 3500 rpm for 30 s. The FTO substrate was sintered at 500 °C for 30 min. The FTO substrate was then dropped with 1 M PbI_2/DMF solution adding with different volume fractions of DMI and then spin-coated at 3000 rpm for 30 s. The PbI_2 precursor film was directly dipped into a solution of CH_3NH_3I (MAI) in 2-propanol with a concentration of 30 mg/mL for 120 s to prepare $MAPbI_3$ films and then annealed at 100 °C for 30 min. A HTM layer was then deposited by spin-coating a solution prepared by dissolving 100 mg spiro-OMeTAD, 40 μL 4-tert-butylpyridine (TBP), 36 μL of a stock solution of 520 mg/mL TFSI in acetonitrile, and 60 μL of a stock solution of 300 mg/mL FK102 dopant in acetonitrile in 1 mL chlorobenzene. Finally, a 60-nm-thick Au film was thermally evaporated on the top of HTM to form a back electrode. The active area of the electrode was fixed at 0.06 cm^2.

Device Characterization

The Lewis adduct of PbI_2·DMI and perovskite films were characterized and evaluated by X-ray diffraction (XRD, Smartlab, Rigaku), field emission scanning electron microscopy (SEM, MERLIN VP Compact), Fourier transform infrared (FTIR) spectroscopy (VERTEX 70v), and thermogravimetric analysis (TGA, Q5000IR). Impedance spectra (IS) of the PSCs were measured in the dark by an electrochemical workstation (CHI660D) under a bias voltage of 0.9 V and an alternative signal of 10 mV in a range from 1 Hz to 1 MHz. Steady-state and time-resolved photoluminescence (PL) spectra were measured by an Edinburgh FLS 920 instrument (Livingston, WL, UK). The current-voltage curves were measured in air illustrated by a solar simulator (AM 1.5G, 100 mW/cm^2, 91195, Newport) at a scan rate of 5 mV/s.

Results and Discussion

Figure 1a, b shows FTIR transmittance spectra of the pure DMF and DMI solvents and their corresponding Lewis adducts. The stretching vibration of C=O bonds is located at 1670 and 1697 cm^{-1} for the DMF and DMI solvents, respectively. When forming Lewis adducts, the C=O peaks separately downshift to 1658 and 1668 cm^{-1}. It indicates that both of the DMI and DMF can interact with PbI_2 through dative Pb–O bonds, which separately form Lewis adducts of PbI_2·DMI and PbI_2·DMF [26, 27]. Figure 1c shows TGA curves of PbI_2 powder and its Lewis adducts of PbI_2·DMI and PbI_2·DMF. The PbI_2·DMF decomposes completely to PbI_2 at 120 °C, while PbI_2·DMI decomposes completely at 200 °C. It indicates that the PbI_2·DMI adduct is more stable than the PbI_2·DMF due to the stronger molecular interaction between DMI and PbI_2. Therefore, it inclines to form PbI_2·DMI when DMI exist in the PbI_2/DMF precursor solution. Figure 1d shows XRD curves of the Lewis adducts of PbI_2·DMI and PbI_2·DMF, which are prepared from PbI_2/DMF solution adding with and without 10 vol% DMI. The PbI_2·DMI has two characteristic diffraction peaks at 7.97° and 9.21°, which are smaller than those of the PbI_2·DMF (9.12° and 9.72°).

When immersed in MAI/2-propanol solution, the Lewis adducts of PbI_2·DMI convert to perovskite through molecular exchange between DMI and MAI basing on following formula:

$$PbI_2 \cdot DMI + MAI \rightarrow MAPbI_3 + DMI \quad (1)$$

Additional file 1: Figure S2 shows XRD curves of the annealed perovskite films prepared by immersing Lewis adducts of PbI_2·DMI in the MAI/2-propanol solution for different times. The XRD peaks at 12.7° and 14.2° are assigned to (001) of the PbI_2 and (110) of the perovskite, respectively [11, 28]. It shows that the PbI_2·DMI converts to perovskite completely within 2 min. There are some residual PbI_2 in the perovskite films when the reaction time is less than 120 s.

Figure 2 shows SEM images of the PbI_2 films and corresponding perovskite films prepared from the PbI_2/DMF solution adding with different amounts of DMI. All the samples are annealed at 100 °C for 30 min before SEM characterization. Compared to DMF, DMI has a higher boiling point and stronger interaction with PbI_2. Therefore, the morphology of the PbI_2 films change evidently with the concentration of DMI. The PbI_2 grains change from ramiform to plate-

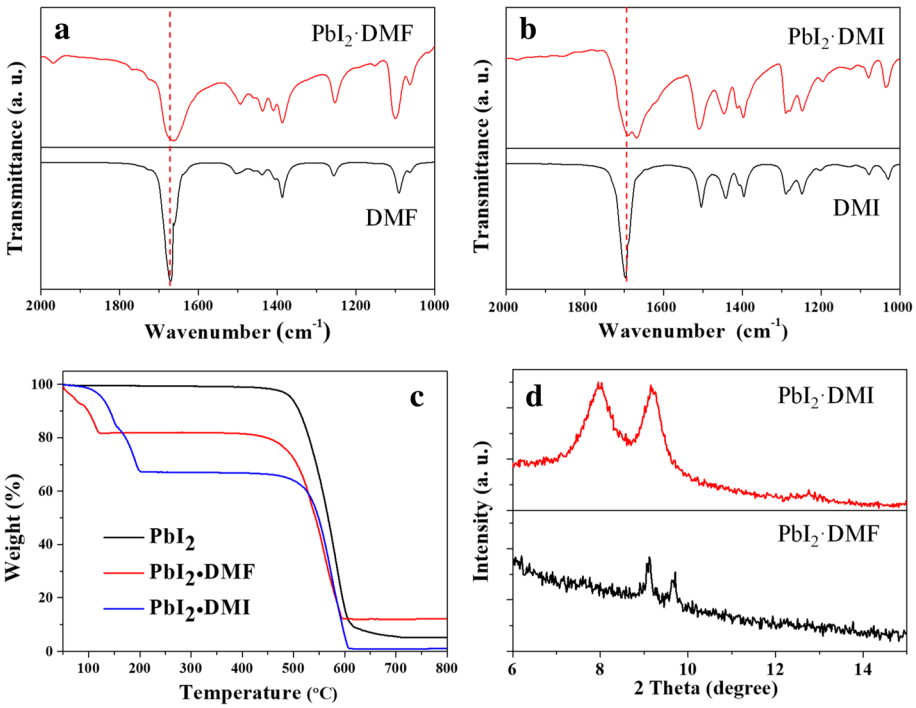

Fig. 1 **a** Fourier transform infrared transmittance spectra of DMF and PbI_2·DMF. **b** Fourier transform infrared transmittance spectra of DMI and PbI_2·DMI. **c** Thermal gravimetric analysis of the PbI_2 Lewis adducts. **d** XRD curves of the Lewis adducts of PbI_2·DMI and PbI_2·DMF

like when 10 vol% DMI is added to the PbI_2/DMF precursor solution (see Fig. 2a, b). However, the PbI_2 films change to porous and even discontinuous, when the DMI concentration increases to 20 vol% (Fig. 2c). The resulting $MAPbI_3$ films are affected by the PbI_2 films significantly. Thus, the perovskite film has a uniform grain and smooth surface for the sample prepared from the solution adding with 10 vol% DMI (see Fig. 2e), which is better than that without DMI. However, excessive DMI might lead to discontinuous

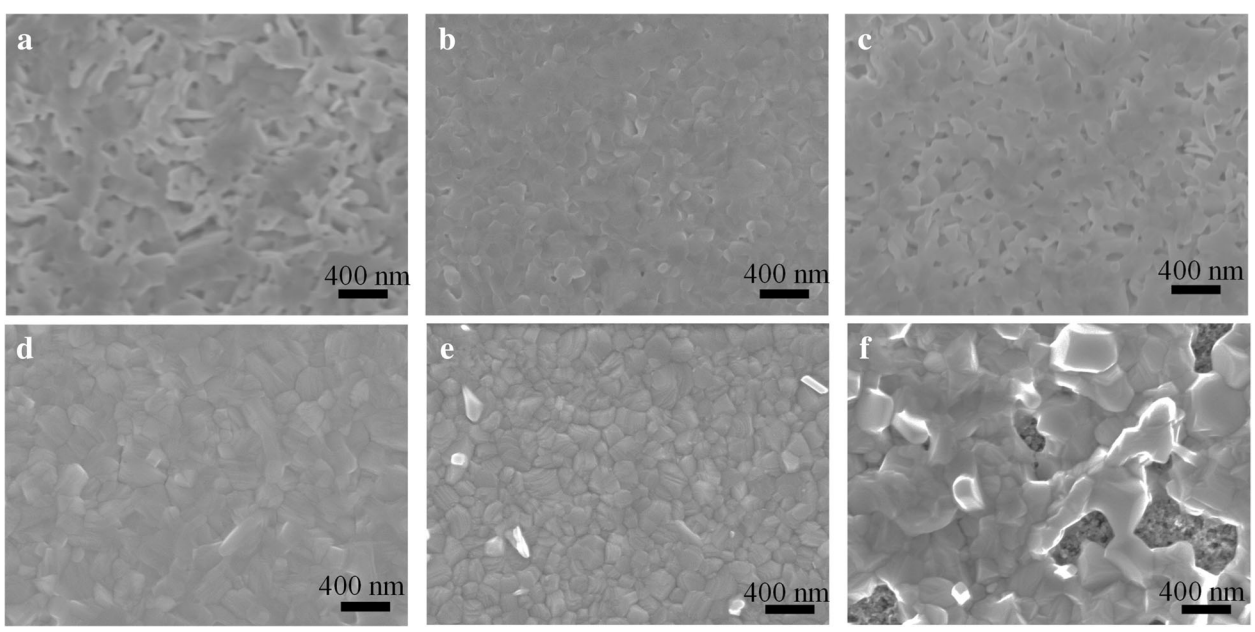

Fig. 2 SEM images of the PbI_2 films (top) and perovskite films (bottom) **a**, **d** without DMI, **b**, **e** 10% DMI, and **c**, **f** 20% DMI

films (see Fig. 2f), which are disadvantageous for the photovoltaic performance of PSCs.

In spite of uniform grain and smooth surface, the grain size of $MAPbI_3$ fabricated from PbI_2/DMF solution with 10% DMI and annealed at 100 °C is not large enough. According to the TGA curves in Fig. 1c, the DMI escapes from the Lewis adducts at higher temperature than the DMF. Herein, we increase the annealing temperature. Figure 3a, b shows top-viewed SEM images of the perovskite films prepared by annealing at 100 and 130 °C from the solution adding with 10 vol% DMI for10 min. It is clear that the grain size increases as the annealing temperature rises. The average grain sizes are 216 and 375 nm for the samples prepared from annealing temperature of 100 and 130 °C, respectively (see Additional file 1: Figure S3). Figure 3c, d shows cross-sectional SEM images of the perovskite solar cells. It shows that the perovskite solar cells have about 250-nm-thick perovskite layers. It contains only one grain in most area for the samples annealed at high temperature (130 °C), which ascribes to the larger grain size than the film thickness. When increasing the annealing temperature to 160 °C, there are some residual PbI_2 in the perovskite films (see Additional file 1: Figure S4), which results in a poor photovoltaic performance (see Additional file 1: Figure S5 the best PCE = 8.53%).

Figure 4a shows J–V curves of the best cells fabricated from the solution adding with different DMI additives. The corresponding photovoltaic parameters are listed in Table 1. The PSCs exhibit the best photovoltaic performance with a PCE of 14.54%, a short current density (J_{sc}) of 21.05 mA/cm^2, an open voltage (V_{oc}) of 1.02 V, and a fill factor (FF) of 67.72% for the samples fabricated from DMF solution adding with 10 vol% DMI and annealing at 130 °C. For the PSCs fabricated from the same precursor solution and annealing at 100 °C, the best PCE is only 12.84%. The PSCs fabricated from the solution with DMI additive have better photovoltaic performances than those from the solution without DMI (the best PCE = 10.72%, J_{sc} = 20.14 mA/cm^2, V_{oc} = 0.97 V, FF = 55.14%). A series of photovoltaic parameters for the PSCs fabricated from different conditions exhibit the similar tendency to the best PSCs as shown in Fig. 4c–f. The devices fabricated from the solution with 10 vol% DMI and annealing at 130 °C exhibit higher PCE than that from the pure DMF. Figure 4b shows an incident photon-to-current efficiency (IPCE) result of a PSC fabricated from DMF solution adding with 10 vol% DMI, which exhibits a good quantum yield. It is noted that the integrated J_{sc} is about 10% lower than that obtained from the reverse scan. This discrepancy might derive from the spectral mismatch between the IPCE light source and solar simulator and from the decay of the devices during the measurement in air [29]. To check the stabilization or saturation point of photocurrent for the PSCs fabricated from the solution with 10 vol% DMI and annealing at 130 °C, we measured the steady-state current of a typical PSC at a bias voltage close to the maximum power point (0.78 V), as shown in Additional file 1: Figure S6a. The PSC

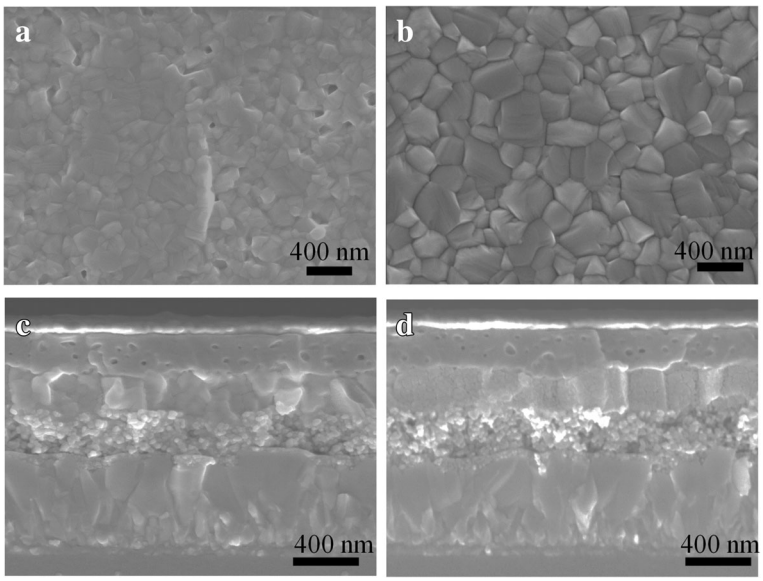

Fig. 3 SEM images of the $MAPbI_3$ films (top) and corresponding perovskite solar cells (bottom). **a**, **c** The perovskite films are prepared from PbI_2/DMF precursor solution adding with 10 vol% DMI and annealing at 100 °C and **b**, **d** at 130 °C

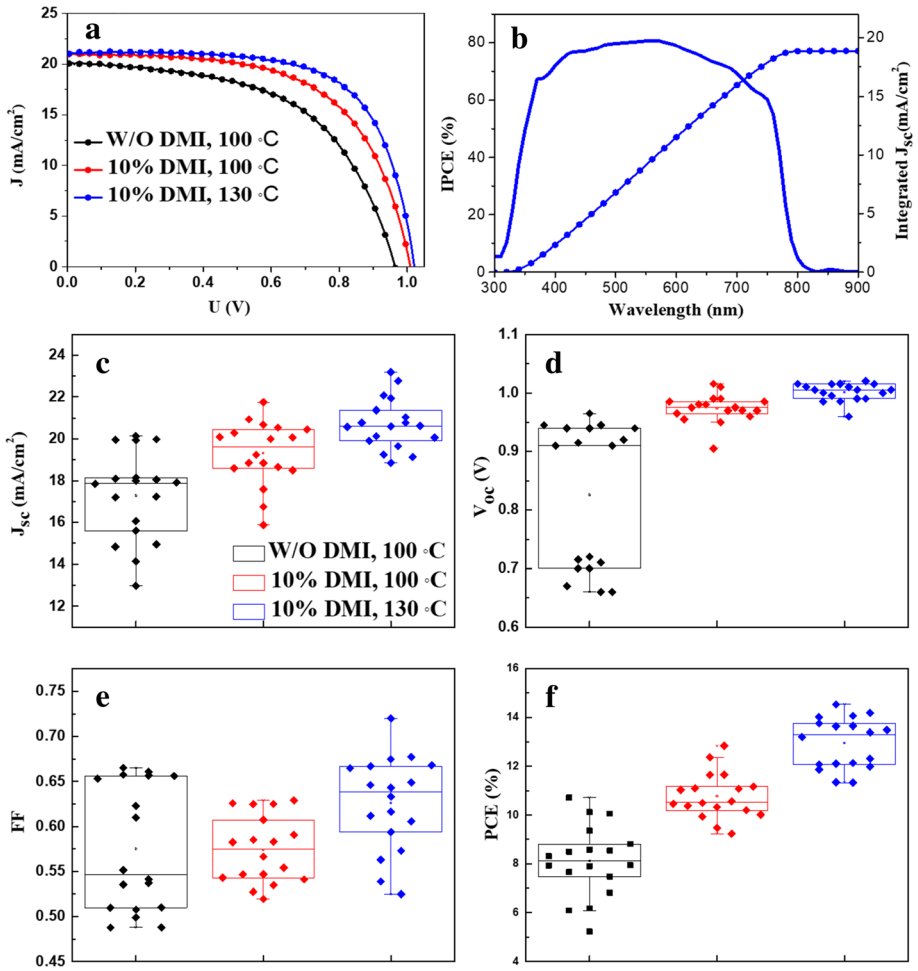

Fig. 4 **a** *J–V* curves of the best PSCs fabricated from different conditions. **b** IPCE spectrum of the best PSCs fabricated from precursor solution adding with 10% DMI and annealing at 130 °C. Box charts of photovoltaic parameters obtained from light *J–V* curves of a series of PSCs. **c** J_{sc}, **d** V_{OC}, **e** FF, **f** PCE

shows a stable output. The device shows an evident hysteresis phenomenon in Additional file 1: Figure S6b.

Figure 5a shows impedance spectra of the PSCs measured in the dark at a forward bias of 0.9 V. The inset of Fig. 5a is an equivalent circuit composed of series resistance (R_s), recombination resistance (R_{rec}) and the transport resistance (R_{HTM}) [30]. The R_s of the PSCs reduces from 26.16 to 14.30 Ω by adding 10% DMI in DMF and annealing at 130 °C compared to without DMI. The small R_s facilitates carrier transport, leading to a high J_{sc} [31]. On the contrary, the R_{rec} increases from 46.49 to 2778 Ω by adding 10 vol% DMI in DMF and annealing at 130 °C compared to pure DMF. The high R_{rec} effectively suppresses the charge recombination for improved device performance.

Figure 5b shows steady-state PL spectra of the $MAPbI_3$ films deposited on mesoporous TiO_2 substrate. The PL spectra are quenched for the perovskite films fabricated from the solution with 10% DMI and

Table 1 Photovoltaic parameters of the best PSCs fabricated from three different conditions

Sample	J_{sc} (mA/cm^2)	V_{oc} (V)	FF (%)	PCE (%)	R_s (Ω)	R_{rec} (Ω)
W/O DMI, 100 °C	20.14	0.97	55.14	10.72	26.16	46.49
10% DMI, 100 °C	20.94	1.01	60.73	12.84	14.65	1206
10% DMI, 130 °C	21.05	1.02	67.72	14.54	14.30	2778

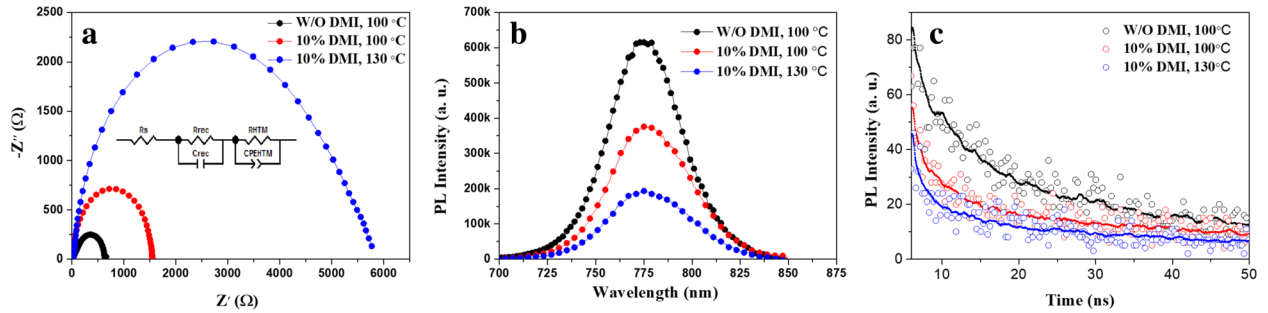

Fig. 5 a Nyquist plots of the perovskite solar cells in the dark at a bias of 0.9 V. **b** Steady PL spectra of the perovskite films. **c** Time-resolved PL spectra basing on the bi-exponential decay function fabricated from three different conditions

annealing at 130 °C, which indicates that the charges transfer effectively from $MAPbI_3$ into a TiO_2 film before they are recombined at the interface for the sample. Compared with those fabricated from the pure DMF, adding some DMI additive can improve the charge transfer. To gain more insight into charge transfer, time-resolved PL of the $MAPbI_3$ films deposited on the mesoporous TiO_2 substrate are also carried out (see Fig. 5c). The spectra are well fitted with a bi-exponential decay function:

$$I(t) = A_1^{\frac{-t}{\tau_1}} + A_2^{\frac{-t}{\tau_2}} \quad (2)$$

where $\tau_1$and τ_2 are the decay time of the two decay processes, respectively. It indicates that there is a fast (τ_1) and a slow (τ_2) decay in the PSCs. The fast decay process is regarded as a quench effect of free carriers in the perovskite film to the electron transport layer (ETL) or HTM, whereas the slow decay process is regarded as the radiative decay [32, 33]. The τ_1 reduces from 3.71 to 2.80 ns when adding 10% DMI and annealing at 100 °C. Furthermore, the τ_1 reduces to 1.90 ns when adding 10% DMI and annealing at 130 °C, demonstrating that the electrons transfer faster from the perovskite film to the TiO_2 ETL layer, as witnessed by stronger steady-state PL quenching. We believe that the enhanced charge transfer rate is ascribed to the increase of large grains and reduce of grain boundary in the perovskite films by adding DMI.

Conclusions

We fabricated high-quality perovskite films with large grains by adding some environmental friendly DMI additives to the PbI_2/DMF solution. It forms a compact Lewis adduct film of PbI_2·DMI, which converts to perovskite films through molecular exchange between DMI and MAI. High-quality perovskite films with large grains are easily obtained by annealing at high temperature. The performances of the perovskite solar cells are thus improved significantly by adding 10 vol% DMI in the precursor solution and annealing at 130 °C.

Additional file

Additional file 1: Figure S1. Molecular structures of DMF and DMI. **Figure S2.** XRD curves of the perovskite films from different immersing times. **Figure S3.** Statistical graphs of the perovskite grains prepared by annealing at different temperatures. (a) 100 °C, (b) 130 °C. **Figure S4.** XRD curves of the perovskite films prepared from three different annealing temperatures. **Figure S5.** *J–V* curve of the best PSC fabricated from DMI solution and annealing at 160 °C. **Figure S6.** (a) Steady-state current measured at the maximum power point (0.78 V), and (b) *J–V* curves under forward (black line) and reverse (red line) scans for a typical perovskite solar cell. (DOCX 295 kb)

Abbreviations

DMF: Dimethylformamide; DMI: 1,3-Dimethyl-2-imidazolidinone; DMSO: *N,N*-Dimethyl sulfox; HMPA: Hexamethylphosphoramide; MAI: CH_3NH_3I; $MAPbI_3$: $CH_3NH_3PbI_3$; NMP: *N*-Methyl pyrrolidone; PSCs: Perovskite solar cells

Authors' Contributions

LLZ, YQL, XBC, YHL, and XC were involved in preparing materials, fabricating devices, and characterizing and measuring. LJC and JQW designed and modified the manuscript. All authors read and approved the final manuscript.

Funding

This work was financially supported by Shenzhen Jiawei Photovoltaic Lighting Co. Ltd., Tsinghua University Initiative Scientific Research Program (20161080165), Scientific Research Program of the Higher Education Institution of Xinjiang (XJEDU2017M038), and National Natural Science Foundation of China (Grant No. 21463002), Natural Science Foundation of Xinjiang Uygur Autonomous Region (No. 2016D01C008), and the Opening Project of State Key laboratory of Crystal Materials (No. KF1610).

Competing Interests

The authors declare that they have no competing interests.

Publisher's Note

Author details

[1]School of Materials Science and Engineering, Shandong University, Jinan 250061, Shandong, People's Republic of China. [2]Department of Physics, Changji College, Changji 831100, Xinjiang, People's Republic of China. [3]Key

Lab for Advanced Materials Processing Technology of Education Ministry, Tsinghua University, Beijing 100084, People's Republic of China. [4]State Key Lab of New Ceramic and Fine Processing, Tsinghua University, Beijing 100084, People's Republic of China. [5]School of Materials Science and Engineering, Tsinghua University, Beijing 100084, People's Republic of China.

Received: 26 October 2017 Accepted: 30 November 2017
Published online: 19 December 2017

References

1. Yang WS, Noh JH, Jeon NJ, Kim YC, Ryu S, Seo J, Seok SI (2015) High-performance photovoltaic perovskite layers fabricated through intramolecular exchange. Science 348:1234–1237
2. Jeon NJ, Noh JH, Yang WS, Kim YC, Ryu S, Seo J, Seok SI (2015) Compositional engineering of perovskite materials for high-performance solar cells. Nature 517:476–480
3. Son DY, Lee JW, Choi YJ, Jang IH, Lee S, Yoo PJ, Shin H, Ahn N, Choi M, Kim D, Park NG (2016) Self-formed grain boundary healing layer for highly efficient $CH_3NH_3PbI_3$ perovskite solar cells. Nat Energy 1:16081
4. Bi D, Yi C, Luo J, Décoppet J-D, Zhang F, Zakeeruddin Shaik M, Li X, Hagfeldt A, Grätzel M (2016) Polymer-templated nucleation and crystal growth of perovskite films for solar cells with efficiency greater than 21%. Nat Energy 1:16142
5. Kim M, Kim G-H, Oh KS, Jo Y, Yoon H, Kim K-H, Lee H, Kim JY, Kim DS (2017) High-temperature-short-time annealing process for high-performance large-area perovskite solar cells. ACS Nano 11:6057–6064
6. Yang WS, Park B-W, Jung EH, Jeon NJ, Kim YC, Lee DU, Shin SS, Seo J, Kim EK, Noh JH, Seok SI (2017) Iodide management in formamidinium-lead-halide–based perovskite layers for efficient solar cells. Science 356:1376–1379
7. Zhang P, Wu J, Wang YF, Sarvari H, Liu DT, Chen ZD, Li SB (2017) Enhanced efficiency and environmental stability of planar perovskite solar cells by suppressing photocatalytic decomposition. J Mater Chem A 5(33):17368–17378
8. Gu XL, Wang YF, Zhang T, Liu DT, Zhang R, Zhang P, Wu J, Chen ZD, Li SB (2017) Enhanced electronic transport in Fe^{3+}-doped TiO_2 for high efficiency perovskite solar cells. J Mater Chem C 5:10754–10760
9. Kim HS, Lee CR, Im JH, Lee KB, Moehl T, Marchioro A, Moon SJ, Humphry-Baker R, Yum JH, Moser JE, Gratzel M, Park NG (2012) Lead iodide perovskite sensitized all-solid-state submicron thin film mesoscopic solar cell with efficiency exceeding 9%. Sci Rep (2):591–597
10. Jeon NJ, Noh JH, Kim YC, Yang WS, Ryu S, Seok SI (2014) Solvent engineering for high-performance inorganic-organic hybrid perovskite solar cells. Nat Mater 13:897–903
11. Wang YF, Wu J, Zhang P, Liu DT, Zhang T, Ji L, Gu XL, Chen ZD (2017) Stitching triple cation perovskite by a mixed anti-solvent process for high performance perovskite solar cells. Nano Energy 39:616–625
12. Ji L, Zhang T, Wang YF, Zhang P, Liu DT, Chen Z, Li SB (2017) Realizing full coverage of stable perovskite film by modified anti-solvent process. Nanoscale Res Lett 12(1):367
13. Burschka J, Pellet N, Moon S-J, Humphry-Baker R, Gao P, Nazeeruddin MK, Gratzel M (2013) Sequential deposition as a route to high-performance perovskite-sensitized solar cells. Nature 499:316–319
14. Leijtens T, Eperon GE, Noel NK, Habisreutinger SN, Petrozza A, Snaith HJ (2015) Stability of metal halide perovskite solar cells. Adv Energy Mater 5: 1500963
15. Yuan S, Qiu Z, Gao C, Zhang H, Jiang Y, Li C, Yu J, Cao B (2016) High-quality perovskite films grown with a fast solvent-assisted molecule inserting strategy for highly efficient and stable solar cells. ACS Appl Mater Interfaces 8:22238–22245
16. Chen H (2017) Two-step sequential deposition of organometal halide perovskite for photovoltaic application. Adv Funct Mater 27:1605654
17. Ahmad S, Kanaujia PK, Niu W, Baumberg JJ, Vijaya PG (2014) In situ intercalation dynamics in inorganic-organic layered perovskite thin films. ACS Appl Mater Interfaces 6:10238–10247
18. Liu D, Gangishetty MK, Kelly TL (2014) Effect of $CH_3NH_3PbI_3$ thickness on device efficiency in planar heterojunction perovskite solar cells. J Mater Chem A 2:19873–19881
19. Zhang H, Mao J, He H, Zhang D, Zhu HL, Xie F, Wong KS, Grätzel M, Choy WCH (2015) A smooth $CH_3NH_3PbI_3$ film via a new approach for forming the PbI_2 nanostructure together with strategically high CH_3NH_3I concentration for high efficient planar-heterojunction solar cells. Adv Energy Mater 5:1501354
20. Li L, Chen Y, Liu Z, Chen Q, Wang X, Zhou H (2016) The additive coordination effect on hybrids perovskite crystallization and high-performance solar cell. Adv Mater 28:9862–9868
21. Ahn N, Son DY, Jang IH, Kang SM, Choi M, Park NG (2015) Highly reproducible perovskite solar cells with average efficiency of 18.3% and best efficiency of 19.7% fabricated via Lewis base adduct of lead (II) iodide. J Am Chem Soc 137:8696–8699
22. Cao XB, Li CL, Zhi LL, Li YH, Cui X, Yao YW, Ci LJ, Wei JQ (2017) Fabrication of high quality perovskite films by modulating the Pb-O bonds in Lewis acid-base adducts. J Mater Chem A 5:8416–8422
23. Zhang Y, Gao P, Oveisi E, Lee Y, Jeangros Q, Grancini G, Paek S, Feng Y, Nazeeruddin MK (2016) PbI_2–HMPA complex pretreatment for highly reproducible and efficient $CH_3NH_3PbI_3$ perovskite solar cells. J Am Chem Soc 138:14380–14387
24. Lee JW, Kim HS, Park NG (2016) Lewis acid–base adduct approach for high efficiency perovskite solar cells. Acc Chem Res 49:311–319
25. Lo CC, Chao PM (1990) Replacement of carcinogenic solvent HMPA by DMI in insect sex pheromone synthesis. J Chem Ecol 16:3245
26. Miyamae H, Numahata Y, Nagata M (1980) The crystal structure of lead (II) iodide-dimethylsulphoxide(1/2). Chem Lett 9:663–664
27. Jungbanger MA, Curran C (1964) N-C=O bending vibration in complexes of dimethylformamide with metal halides. Nature 202:290
28. Hwang I, Jeong I, Lee J, Ko MJ, Yong K (2015) Enhancing stability of perovskite solar cells to moisture by the facile hydrophobic passivation. ACS Appl Mater Interfaces 7:17330–17336
29. Cao XB, Li YH, Fang F, Cui X, Yao YW, Wei JQ (2016) High quality perovskite films fabricated from Lewis acid-base adduct through molecular exchange. RSC Adv 6:70925–70931
30. Cao XB, Li CL, Li YH, Fang F, Cui X, Yao YW, Wei JQ (2016) Enhanced performance of perovskite solar cells by modulating the Lewis acid-base reaction. Nano 8:19804–19810
31. Yang D, Yang R, Zhang J, Yang Z, Liu S, Li C (2015) High efficiency flexible perovskite solar cells using superior low temperature TiO_2. Energy Environ Sci 8:3208–3214
32. Mali SS, Shim CS, Kim H, Patil PS, Hong CK (2016) In situ processed gold nanoparticle-embedded TiO_2 nanofibers enabling plasmonic perovskite solar cells to exceed 14% conversion efficiency. Nano 8:2664–2677
33. Zhao X, Shen H, Zhang Y, Li X, Zhao X, Tai M, Li J, Li J, Li X, Lin H (2016) Aluminum-doped zinc oxide as highly stable electron collection layer for perovskite solar cells. ACS Appl Mater Interfaces 8:7826–7833